Tulips R
University of Tsukuba Repository

Cross-sectional particle measurement in the resonance domain on the substrate through scatterometry

著者	Hoshino Tetsuya, Watanabe Norio, Aoki Sadao, Sakurai Kenji, Itoh Masahide
journal or publication title	Optics express
volume	25
number	21
page range	26329-26348
year	2017-10
権利	(C) 2017 Optical Society of America. Users may use, reuse, and build upon the article, or use the article for text or data mining, so long as such uses are for non-commercial purposes and appropriate attribution is maintained. All other rights are reserved.
URL	http://hdl.handle.net/2241/00148685

doi: 10.1364/OE.25.026329

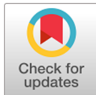

Research Article Vol. 25, No. 21 | 16 Oct 2017 | OPTICS EXPRESS 26329

Optics EXPRESS

Cross-sectional particle measurement in the resonance domain on the substrate through scatterometry

TETSUYA HOSHINO,[1,*] NORIO WATANABE,[1] SADAO AOKI,[1] KENJI SAKURAI,[2] AND MASAHIDE ITOH[1]

[1]*Institute of Applied Physics, University of Tsukuba, 1-1-1 Tennoudai, Tsukuba 305-8577, Japan*
[2]*National Institute for Materials Science, 1-2-1 Sengen, Tsukuba, Ibaraki, 305-0051 Japan*
**hoshino.tetsuya.gt@u.tsukuba.ac.jp*

Abstract: We developed a versatile method for three-dimensional shape measurement where a specific particle can be selected on the substrate and its cross-sectional shape and size can be measured. A non-contact fast measurement is possible for the particle in the resonance domain. We applied rigorous coupled-wave analysis to the particle and calculated the diffraction patterns, comparing the patterns with the experimental results to obtain the size and shape. The shape and position of the focusing spot on the scattering particle was controlled precisely. With this method, the category of the analyzable object is extended to more shapes, such as rectangles and triangles, in addition to a conventional ellipsoid.

© 2017 Optical Society of America

OCIS codes: (290.5820) Scattering measurements; (050.5745) Resonance domain; (110.6880) Three-dimensional image acquisition; (120.3930) Metrological instrumentation.

References and links

1. Malvern Instruments, "Automated imaging advanced particle characterization," http://www.malvern.com/Assets/MRK1900.pdf. Accessed: 2017–03–03.
2. M. Umezawa and H. Sugasawa, "The LA-960 Laser Diffraction/Scattering Particle Size Distribution Analyzer," Readout: Horiba technical reports pp. 92–96 (2013).
3. K. S. Al-Rubaie, H. N. Yoshimura, and J. D. B. de Mello, "Two-body abrasive wear of Al–SiC composites," Wear **233**, 444–454 (1999).
4. A. Kuriyama and Y. Ozaki, "Assessment of active pharmaceutical ingredient particle size in tablets by Raman chemical imaging validated using polystyrene microsphere size standards," AAPS PharmSciTech **15**(2), 375–387 (2014).
5. A. Devaney, "Current research topics in diffraction tomography," *Inverse Problems in Scattering and Imaging* (CRC Press, 1992), pp.47–58.
6. P. Muller, M. Schurmann, and J. Guck, "The theory of diffraction tomography," arXiv preprint arXiv:1507.00466 (2015).
7. K. Sakurai and M. Mizusawa, "X-ray diffraction imaging of anatase and rutile," Anal. Chem. **82**(9), 3519–3522 (2010).
8. M. Sperazza, J. N. Moore, and M. S. Hendrix, "High-resolution particle size analysis of naturally occurring very fine-grained sediment through laser diffractometry," J. Sediment. Res. **74**, 736–743 (2004).
9. A. Taguchi, T. Miyoshi, Y. Takaya, and S. Takahashi, "Optical 3D profilometer for in-process measurement of microsurface based on phase retrieval technique," Precis. Eng. **28**, 152–163 (2004).
10. H. E. Exner, "Stereology and 3D microscopy: useful alternatives or competitors in the quantitative analysis of microstructures?" Image Anal. Stereol. **23**, 73–82 (2011).
11. D. P. Kelly, B. M. Hennelly, N. Pandey, T. J. Naughton, and W. T. Rhodes, "Resolution limits in practical digital holographic systems," Opt. Eng. **48**, 095801 (2009).
12. M. J. Berg, S. C. Hill, Y.-L. Pan, and G. Videen, "Two-dimensional Guinier analysis: application to single aerosol particles in-flight," Opt. Express **18**(22), 23343–23352 (2010).
13. T. Nousiainen, M. Kahnert, and H. Lindqvist, "Can particle shape information be retrieved from light-scattering observations using spheroidal model particles?" J. Quant. Spectrosc. Radiat. Transf. **112**, 2213–2225 (2011).
14. P. Barber and C. Yeh, "Scattering of electromagnetic waves by arbitrarily shaped dielectric bodies," Appl. Opt. **14**(12), 2864–2872 (1975).
15. B. W. Fowler and C. C. Sung, "Scattering of an electromagnetic wave from dielectric bodies of irregular shape," J. Opt. Soc. Am. **69**, 756–761 (1979).
16. D. W. Schuerman, R. T. Wang, B. A. S. Gustafson, and R. W. Schaefer, "Systematic studies of light scattering. 1: Particle shape," Appl. Opt. **20**(23), 4039–4050 (1981).

#306331 https://doi.org/10.1364/OE.25.026329
Journal © 2017 Received 4 Sep 2017; accepted 4 Oct 2017; published 13 Oct 2017

17. M. Mishchenko, L. Travis, and A. Lacis, *Scattering, Absorption, and Emission of Light by Small Particles* (Cambridge University Press, 2002).
18. T. Nousiainen, "Impact of particle shape on refractive-index dependence of scattering in resonance domain," J. Quant. Spectrosc. Radiat. Transf. **108**, 464–473 (2007).
19. A. G. Hoekstra, M. Grimminck, and P. M. Sloot, "Simulating light scattering from micron-sized particles," in "International Conference on High-Performance Computing and Networking," (Springer, 1996), pp. 269–275.
20. H. Lindqvist, O. Jokinen, K. Kandler, D. Scheuvens, and T. Nousiainen, "Single scattering by realistic, inhomogeneous mineral dust particles with stereogrammetric shapes," Atmos. Chem. Phys. **14**, 143–157 (2014).
21. D. A. Pommet, M. G. Moharam, and E. B. Grann, "Limits of scalar diffraction theory for diffractive phase elements," J. Opt. Soc. Am. A **11**, 1827–1834 (1994).
22. S. Iwasaki and H. Okamoto, "Analysis of the enhancement of backscattering by nonspherical particles with flat surfaces," Appl. Opt. **40**(33), 6121–6129 (2001).
23. M. A. Golub and A. A. Friesem, "Analytic design and solutions for resonance domain diffractive optical elements," J. Opt. Soc. Am. A **24**(3), 687–695 (2007).
24. T. Hoshino, S. Banerjee, M. Itoh, and T. Yatagai, "Design of a wavelength independent grating in the resonance domain," Appl. Opt. **46**(32), 7942–7956 (2007).
25. K. Chakrabarti and J. B. Cole, "Simulation study on the detection of size, shape and position of three different scatterers using non-standard time domain time inverse Maxwell's algorithm," Opt. Express **18**(5), 4148–4157 (2010).
26. V. Myroshnychenko, E. Carbo-Argibay, I. Pastoriza-Santos, J. Perez-Juste, L. M. Liz-Marzan, and F. J. Garcia de Abajo, "Modeling the optical response of highly faceted metal nanoparticles with a fully 3D boundary element method," Adv. Mater. **20**, 4288–4293 (2008).
27. J. I. Hage, J. M. Greenberg, and R. T. Wang, "Scattering from arbitrarily shaped particles: theory and experiment," Appl. Opt. **30**(9), 1141–1152 (1991).
28. T. Hoshino and M. Itoh, "Cross-sectional shape evaluation of a particle by scatterometry," Opt. Commun. **359**, 240–244 (2016).
29. M. G. Moharam and T. K. Gaylord, "Rigorous coupled-wave analysis of grating diffraction E-mode polarization and losses," J. Opt. Soc. Am. A **73**, 451–455 (1983).
30. H. Shapiro, *Practical flow cytometry* (Wiley-Liss, 2003).
31. A. Abdelmonem, M. Schnaiter, P. Amsler, E. Hesse, J. Meyer, and T. Leisner, "First correlated measurements of the shape and light scattering properties of cloud particles using the new particle habit imaging and polar scattering (PHIPS) probe," Atmos. Meas. Tech. **4**, 2125–2142 (2011).
32. A. Jones, "Light scattering for particle characterization," Prog. Energ. Combust. **25**, 1–53 (1999).
33. A. Guinier and G. Fournet, *Small Angle Scattering of X-Rays* (J. Wiley & Sons, 1955).
34. S. G. Warren, "Optical constants of ice from the ultraviolet to the microwave," Appl. Opt. **23**(8), 1206–1225 (1984).
35. W. Xu, M. H. Jericho, H. J. Kreuzer, and I. A. Meinertzhagen, "Tracking particles in four dimensions with in-line holographic microscopy," Opt. Lett. **28**(3), 164–166 (2003).
36. M. Born and E. Wolf, *Principles of Optics: Electromagnetic Theory of Propagation, Interference and Diffraction of Light* (Cambridge University Press, 1999), 7th ed.
37. T. Hoshino, M. Itoh, and T. Yatagai, "Antireflective grating in the resonance domain for displays," Appl. Opt. **46**(5), 648–656 (2007).
38. Y. Wu, X. Wu, L. Yao, M. Brunel, S. Coëtmellec, D. Lebrun, G. Gréhan, and K. Cen, "3d boundary line measurement of irregular particle with digital holography," Powder Technol. **295**, 96–103 (2016).
39. T. Murakami, "A new direct analysis method for measuring particle size and location by inline hologram," in *Laser Diagnostics and Modeling of Combustion* (Springer, 1987), pp. 71–76.
40. M. Born and E. Wolf, *Principles of Optics: Electromagnetic Theory of Propagation, Interference and Diffraction of Light* (Cambridge University Press, 1999), 7th ed.
41. J. C. Wyant and K. Creath, "Basic wavefront aberration theory for optical metrology," Applied optics and optical engineering **11**, 28–39 (1992).
42. T. Hoshino, T. Yatagai, and M. Itoh, "Precise and rapid distance measurements by scatterometry," Opt. Express **20**(4), 3954–3966 (2012).
43. T. Hoshino, M. Itoh, and T. Yatagai, "Scatterometry of Slant Incidence to Isolated Scatterers for High-Density Memory," Jpn. J. Appl. Phys. **52**, 09LA05 (2013).
44. T. Hoshino, S. Banerjee, M. Itoh, and T. Yatagai, "Diffraction pattern of triangular grating in the resonance domain," J. Opt. Soc. Am. A **26**(3), 715–722 (2009).
45. T. Smith, M. Irwanto, D. Haines, K. Ghiggino, and D. Millar, "Time-resolved fluorescence anisotropy measurements of the adsorption of rhodamine-b and a labelled polyelectrolyte onto colloidal silica," Colloid Polym. Sci. **276**, 1032–1037 (1998).

1. Introduction

Two- or three-dimensional (2D or 3D) shapes and sizes of many particles on a substrate are measured using commercially available optical methods, and the size distribution is calculated [1, 2]. This technique is applied to analyze abrasives, drag component, etc [3, 4].

Instead of lens microscopy, diffraction tomography is sometimes used [5–8], and is suitable for the measurement of moving particles because of its wide focusing range.

The precision of the conventional method does not reach diffraction limit for a 3D single particle with a size of several wavelengths when the refractive index difference between the particle and its surroundings is approximately more than 0.3. This region is called the resonance domain, whose size is 0.5–10 wavelengths. In addition, the diffraction in this region is strong and the light does not pass straight through the particle.

One of the reasons for this problem could be that the distance between front and back surfaces is difficult to estimate due to the disturbance of diffraction. The 3D surface shape can be measured through holography or stereography [9–11]. Phase distortion due to the back surface severs the interference of these methods.

To overcome this problem, a scattering pattern should be analyzed through rigorous simulation. Hitherto, the analyzable unknown shape was limited to an ellipsoid and the surroundings were required to be homogeneous [12–16]. For the simulation, the T-matrix method and dipole–dipole method are frequently used because they can treat various shapes easily [17–20]. We surveyed and determined that the influence of polarization on particle scattering in the resonance domain is considerable [21–24]. Therefore, we decided to use a wave-vector simulation method, which can consider polarization by itself. The finite difference time domain (FDTD) method, boundary element method (BEM), volume integral equation formulation (VIEF), and rigorous coupled-wave analysis (RCWA) are popular for such a simulation [25–28]. In this study, we used the RCWA because it utilizes a small amount of time for setting various shapes and is suitable for far-field calculation [29].

To resolve the above-mentioned problem of bad resolution in particle measurement caused by phase distortion in the resonance domain, we developed a new method to measure the 3D shape and size of the scatterer with the help of the scattering pattern and simulation. In this method, RCWA is used for the estimation of particle width [28].

For the experiment, isolation of a single particle is favorable for the analysis of a scattering pattern; thus liquid or air flow is a representative method [12, 30–32]. In this study, we set particles on a substrate so that the experiment can be performed in various conditions, such as in a vacuum system, though the analysis should consider the effect of the substrate on the diffraction pattern of a particle. The diffraction pattern of a particle in the air should differ from that of a particle on the substrate.

In addition to a proper simulation method, we determined the rule that tells the shape of the particle from the diffraction pattern. If the particle is an isolated cylinder or a flat circular disc, the scattering pattern can be analyzed using the Guinier plot [12, 33], which relates the scattering pattern to the shape and size.

Realistically, as particle shapes and diffraction patterns have many relations, an entire 3D diffraction pattern cannot be analyzed in one step. We projected a line pattern onto the particle to observe the cross-sectional shape. In addition, we constructed a 3D image from this 2D shape. This method may work properly only when most of the light is diffracted in the same plane including the optical axis and focused line. To solve this problem, we adjusted the position of the projected linearly shaped light so that it crossed the center of the particle's diffraction image.

If the particle flows and the distance between particles is large, we can easily identify one of the particles. However, because the particles here are neighbors, they should be resolved and identified. To solve this problem, we used a focusing lens for the incident light. However, this caused the diffraction pattern to change considerably with respect to the distance between the focal point and particle, and the determination of the precise distance seems difficult. We arrived at a solution to this problem.

We determined the characteristics of the diffraction pattern that would enable us to distinguish between triangles, rectangles, and ellipsoids and to determine the aspect ratio.

Optics EXPRESS

The above-mentioned method is useful when the diffraction effect is strong, which would complicate the determination of a cross-sectional shape as well as the surface shape or shape of a hidden particle. By considering the refractive index difference between the particle and air, the applicable wavelength was determined to range from a soft X-ray to microwave [34]. The precise and rapid measurement of a particle's dimensions through soft X-ray or in the visible region is the most suitable. In a soft X-ray region, focusing a lens to the wavelength order is difficult and in the visible region, available wavelength range is limited.

2. Principle and method

2.1. Focal distance and diffraction pattern

We located one of the particles present on a slide glass. The cross section was then selected from the particle, and the diffraction pattern of the particle was observed on the screen. The basic mechanism is shown in Fig. 1.

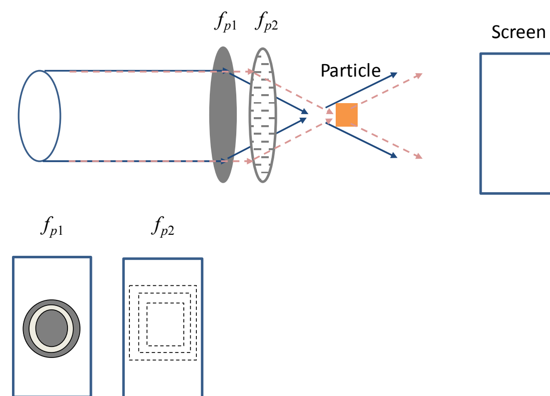

Fig. 1. Lens-particle distances f_{p1}, f_{p2} and the diffraction patterns on the screen.

When lens-particle distance f_p is longer than focal length, the diffracted light and the not-diffracted light of a particle interfere, and the system makes in-line hologram of the particle [35]. When lens-particle distance f_p is just near focal length and aberration is small enough, all light is condensed near the particle, and only the diffraction pattern is observed. Thus, it is important to control the distance f_p. We noticed that the in-line hologram seemed concentric circles, whatever the particle shape was either circle or rectangle, as shown later. The difference of the pattern is also illustrated in Fig. 1.

NA (Numerical Aperture) is known as the parameter which regulates the minimum focusing diameter [36]. When the diameter of the pupil becomes smaller, its NA becomes smaller, and the focusing spot becomes larger. We used a variable slit to use this effect of NA. The shape of focusing spot becomes vertical rectangle, when the slit shape is horizontal rectangle [36]. We used this long and narrow beam spot for selecting the cross section of the 3D particle.

The converging beam is not favorable to the analysis of the diffraction pattern, but it is necessary to use the converging beam to select one particle from the others. If parallel light is not to be used and the light is converging, the diffraction pattern becomes broad and the angular resolution of the diffraction pattern is lowered. To avoid this problem, we used a slit so that angle range of incident light is narrowed and this broadening is suppressed. The analysis is performed along the axis of the narrower aperture of the slit. In this way, the incident light is assumed to be parallel, and we can simulate the diffraction pattern by parallel light.

Optics EXPRESS

2.2. Resonance domain and diffraction pattern

The diffraction pattern and reflectivity of the particle in the resonance domain change by size and shape much more sensitively than those out of resonance domain [37]. The mechanism is explained by the complex reflection and interference of light in the particle [24]. The simple phase analysis by inline-hologram is expected to be difficult. In fact, if the size is several thousand wavelengths, the irregular shape was analyzed [38]. However, if the size is several ten wavelengths, the analyzable particle shape is limited to sphere [39]. To resolve this problem, we observed and analyzed the diffraction pattern itself.

2.3. Experiment procedure

The details are as follows. The diffraction pattern of the particle is measured by a system (Fig. 2), which is made of a light source, lens, particles on the slide glass, and a screen. The light source is an Ar ion laser (Spectra-Physics Stabilite, 2017) with a wavelength of 488 nm. It is reflected by a mirror twice to change its direction and height. The polarization-beam splitter sets the electric field oscillation along the y-axis. In this study, we define this mode of light as transverse magnetic (TM). When the electric field oscillates along the x-axis, we define its polarization as the transverse electric (TE) mode. A pin hole with diameter 1 μm is used as a spatial filter. The iris diaphragm and variable slit are set to shape the beam spot. The variable slit can rotate around the optical axis. The width of its opening is 1 mm and its height is 2 cm. Furthermore, the focal length of the lens is 5 cm. The particles are spread on to the slide glass by n-Hexane, which evaporates immediately. The particle is Rhodamine B, with 90% pureness provided by Aldrich Chem. In addition, the n-Hexane special grade is provided by Wako Pure Chem. The slide glass is a Matsunami white glass G1111 with a thickness of 0.8 mm. The position of the slide glass was adjusted through a micrometer, and it can rotate around the x-axis. To change the rotation axis of the particle, the slide glass was removed from the stage, rotated around the z-axis, and set again. The diffraction pattern is projected onto a white Ricoh A4 size TP paper (210 mm × 297 mm) and is captured using a digital Olympus STYLUS XZ-10 camera, whose shutter speed and diaphragm are changed automatically with the brightness. The effect of the slit width on the diffraction pattern was observed by changing the slit width; however, we ensured that the effect was small. When the slit was parallel to the y-axis, we defined the rotation angle of slit as 0°. The distance between the particle and focal point was manually adjusted with micrometer precision. The position of the particle in the xy-plane was adjusted similarly.

To set the distance between the focal point and particle, the distance was adjusted so that the contrast in the diffraction pattern was the highest. As shown later, we determined that the distance could be set at a unique point experimentally; this was ensured through a simulation.

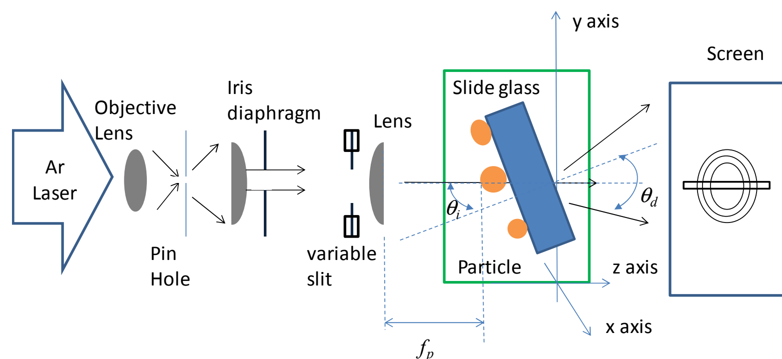

Fig. 2. Scattering measurement by using an Ar laser (488 nm): f_p is the distance between the lens and particle.

Optics EXPRESS

The procedure to focus on a specific particle is as follows. As shown in Fig. 2, first we opened the iris diaphragm wide and removed a variable slit so that a large area was illuminated. We searched for the destination particle by using markers painted using dotted ink with 1 mm intervals. Then the distance f_p is adjusted so that the contrast of image on the screen becomes highest. In the next, the aperture of iris diaphragm is narrowed to reduce the aberration [40, 41]. Finally, a slit is inserted to shape the focusing spot line and select cross section of the 3D particle. The rectangle on the screen is the projection of the slit in Fig. 2.

The image of the particle was viewed through an optical microscope OLYMPUS BX51 with an objective lens 10 × /0.25 NA and an eyepiece WH10 × /22.

2.4. Analysis procedure

We utilized the relationship between the angular distribution periodicity and width w to calculate the size of the scatterer [28]. For the diffraction angle θ, refractive index of air n_0, diffraction order m, and wavelength λ, the width w of the particle is given by

$$w = m\lambda \div \left[n_0 \sin(\theta) \right] \tag{1}$$

Although this is a first-order approximation, we used this value for shape and size estimation.

The simulation of diffraction pattern by using RCWA is mentioned in a previous paper [42]. The program is DiffractMOD^{TM} 1.5(RSoft Design Group, Ossining, NY, USA). We have made experiment and compared the results with simulation to make the bases to apply RCWA to an isolated particle [24, 43]. There is no limitation on the simulatable shape, and the time to make the source data does not depend on the shape very much. The limitation is posed by the computer’s ability and it restricts the size of the particle and the number of space dimensions.

3. Result

First, the particles are observed at a low magnification, and the specified particle P2 is focused by moving the focusing lens toward P2 (Figs. 3(a) and 3(b)). The diffraction intensity clued us to the particle size. The opening of the iris diaphragm was narrowed to 6 mmϕ to cut the nonfocused light (Fig. 3(c)). The pattern suggests the rough outline of the particle. To shape the focusing spot line, a slit with 1 mm width was inserted (Fig. 3(d)).

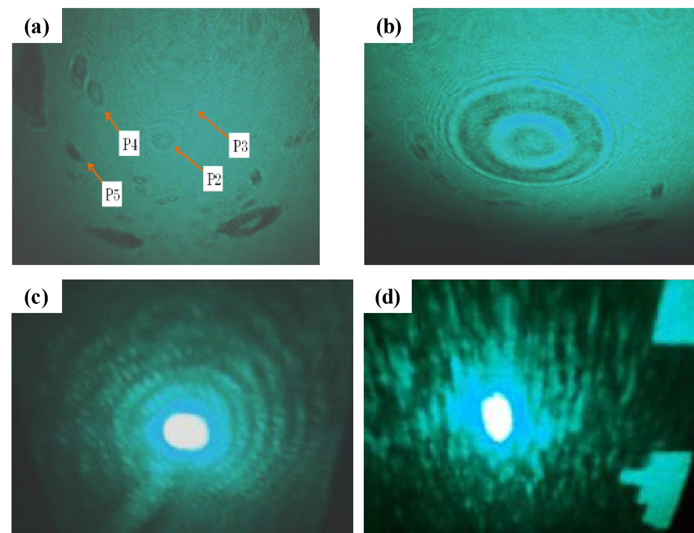

Fig. 3. Scattering patterns of the particles: (a) Particles P2, P3, P4, and P5. (b) Zoomed up P2. (c) Iris diaphragm applied to P2. (d) Slit and iris diaphragm applied to P2.

Optics EXPRESS

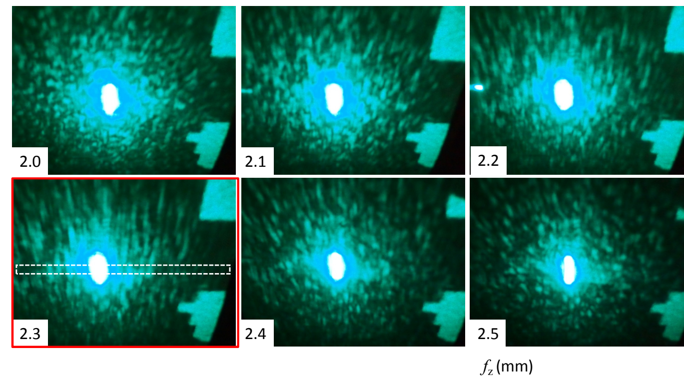

Fig. 4. Scattering patterns of particle P2, to which the slit and iris diaphragm are applied. The focusing lens was moved from P2. The analyzed part for angular distribution is indicated by dotted line. The bright area at the right hand of each picture is the strayed beam of light source.

In the experiment, the distance f_p may significantly affect the diffraction pattern. Thus, it is important to control this distance accurately to achieve repeatability. We analyzed the change in the diffraction pattern with f_z (Fig. 4). Here, $f_z = f_p - f_0$, and $f_0 = 5$ cm. As a result, when we moved the focusing point to the particle, we found the highest contrast diffraction at a certain point ($f_p - f_0 = 2.3$mm). f_0 is the value of f_p when the memory of the micrometer is 0. The distinct diffraction patterns of particles P1–P5 are measured. The measured data include diffraction patterns, such as those shown in Fig. 3(c) and 3(d). In the data, variable slits are rotated around the z-axis. The rotation angle θ_r was taken as 0°, 45°, 90°, and 135° for incident angle $\theta_i = 0°$. Only P1 has additional data of $\theta_r = 90°$ and incident angle $\theta_i = 0°$, 15°, 30°, and 45°. The data of other particles contains $\theta_r = 90°$ and incident angle $\theta_i = 45°$. The distance between the slide glass and the screen is 95 mm for P1 and 192 mm for P2–P5. As the size of P1 is small, a large diffraction angle should be observed (See Eq. (1)). The image of the screen is captured from the side of the light source except for P1. As the space for the camera work is small for P1, the image could not be captured from the front side, and therefore it was captured from the back side of the screen.

Figure 4 shows the highest contrast pattern at a unique distance. It is important to obtain repeatable results. We verified this result through simulation of RCWA. Figure 5 shows the simulation scheme, in which the planar incident light is focused on a square particle on the board. The focal length is 50λ, and distance from lens to particle is f_p. Actually, in the simulation, $f_0 = 0$ and $f_z = f_p$. The refractive index of all components, except the shading plate with thickness d, was set to 1.5. The shading plate has the thickness $d = \lambda$ and its complex refractive index is 1.5 + 3i. The diffraction angle is represented by θ_d, with polarization TE. In the experiment, focusing light in the xz plane is TE and focusing light in the yz plane is TM. Moreover, the thickness of the board is assumed to be infinite to remove the effect of reflection of back side of the board and to make the analysis simple.

Due to the restriction of computer performance, the diameter of the lens becomes 24λ, which is much smaller than the focusing lens used in the experiment. To make sure of the focusing effect, we calculated electric field by RCWA for the optical system in Fig. 5 (See Fig. 12 in appendix). The width of square particle is 6λ. There is normal focusing effect and we used this system for the next simulation of diffraction.

Figure 6 illustrates the result of diffraction pattern to calculate the contrast. The particle is square-shaped with a width of 6λ. The highest contrast pattern emerges for diffraction angle ranging from 8° to 20° when f_p comes closer to the focal length. The corresponding valley and peak are indicated by arrows. The range of the corresponding peak is set from 8° to 15° and the range of the valley is set from 13° to 20°. The intensity of the peak is I_{max} and that of the valley is I_{min}. The contrast is defined as the intensity ratio I_{max} / I_{min}. The particles are

Optics EXPRESS

simulated for three shapes and for three widths 2λ, 6λ, and 10λ (See appendix, Figs. 13–14). The three shapes are circle, isosceles triangle, and square. The height of the triangle is same to its base length.

These figures show that there is local maximum, when focal point is near the particle. Thus, by the simulation we could show the existence of maximum contrast against f_z, which was already indicated in the experiment. Though the lens size and focal length is different from the experiment, we can say at least the phenomenon is usual.

It seems that the electric field is parallel to the optical axis in front of the particle in Fig. 12. To check the effect of lens size, we also calculated the lens with width 18λ and 30λ. In both cases of the widths, the light is focused in front of the particle when f_p is 50λ. For three lenses' widths, the contrast of the diffraction pattern becomes maximum, when f_p is near 50λ. The above calculations for contrast of diffraction pattern was performed in TE mode, but we also got the similar result in TM mode.

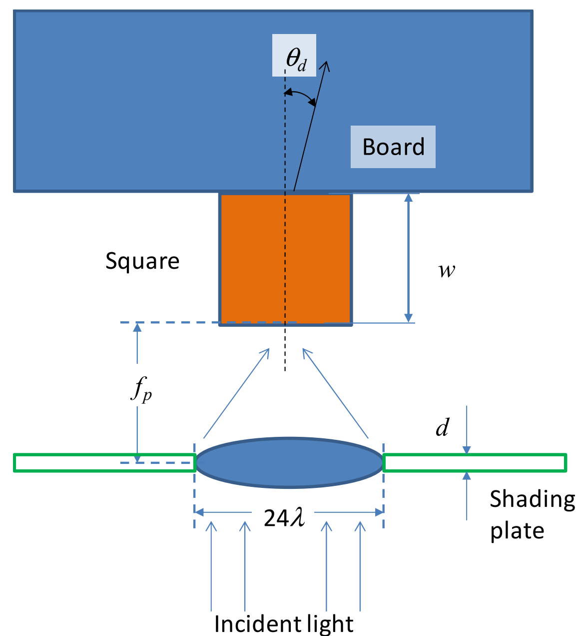

Fig. 5. Scheme of the optical system for simulation. Diffraction angle is θ_d.

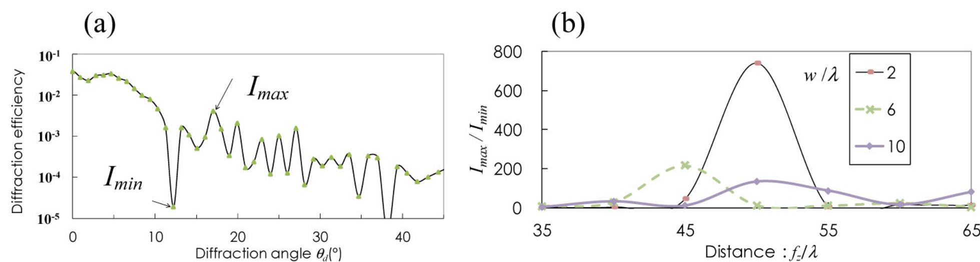

Fig. 6. Scattering pattern and its analysis simulated using RCWA for a square. [$f_z = f_p$] (a) Scattering pattern with width w = 6λ and distance f_z = 45λ, and (b) its contrast analysis by I_{max}/I_{min} for different f_z.

Figure 4 shows the analyzed area of the diffraction pattern indicated by a dotted line. The diffraction angle is derived from the screen width and distance between the screen and particle. Figure 7 shows the diffraction pattern for particle P1 with incident angle of 0°–45°.

The diffraction pattern seems to have a flat area from −10° to 10° when θ_i = 0°. This might be due to the reflection on the back surface of the slide glass. Next, we considered the effect in simulation; however, the thickness of the glass was considerably large. Therefore, we surveyed whether it is possible to use a tentatively thin slide glass instead of a real slide glass for simulation. The particle has a circular shape, with polarization TE or TM, and diameter = 3λ, 5λ, 10λ or 20λ. The thickness of the slide glass was 10λ or 20λ. Thus, the thickness has an insignificant effect on the diffraction pattern (See appendix, Fig. 15).

We decided to calculate the diffraction pattern to simulate those of particles P1–P5 with thickness 13.1λ (Fig. 8). The thickness is not set to an integer to have little interference effect.

To search the way to derive the shape and size, let's analyze the diffraction of P1 in Fig. 7 as an example. At first, we estimated the width of P1 to be 3λ according to Eq. (1) when θ_i = 0° and θ_r = 90°. The diffraction pattern of P1 with θ_i = 0° has peaks at around ± 35°. Next, we payed attention to the peaks at ± 35° and calculated diffraction patterns by changing the shape and aspect ratio. Figure 8 shows the scheme of simulation for this. The particles' aspect ratio ($r_{asp} = d/w$) is 0.2, 0.4, 0.6, 0.8, or 1. We searched the three shapes which could have peaks at ± 35°. Figure 9 gives the diffraction patterns similar to that of experiment. We estimated the particle's shape to be a triangle as the peak space was not constant when incident angle varied and broadening occurred when the incident angle was 45°. When we compare the diffraction pattern of three shapes in Fig. 9, the broad peak at around 10-30° is the feature of the triangle and can be the criteria to estimate the shape, as mentioned later. This is supported by the theory that the diffraction pattern of the triangle in the resonance domain has two peaks whose angle can be predicted from the geometric optics [44].

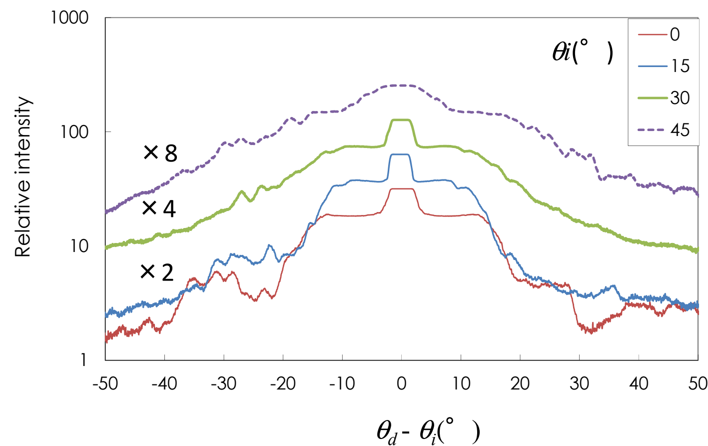

Fig. 7. Horizontal projection profile of the diffraction pattern of particle P1. θ_i = 0°, 15°, 30°, and 45°.

Optics EXPRESS

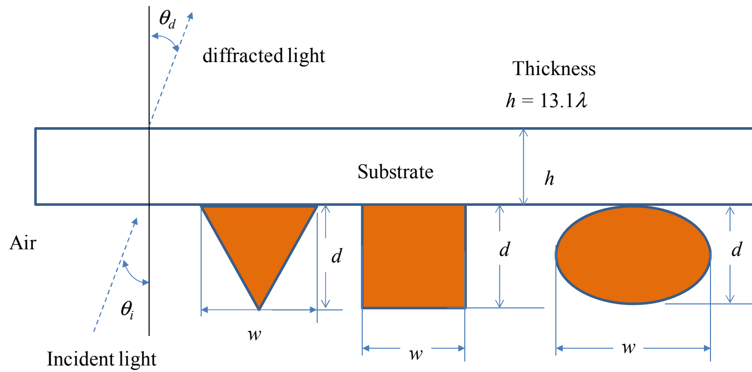

Fig. 8. Optical system of simulation for three types of particles. Particles and a substrate have same refractive index of 1.5.

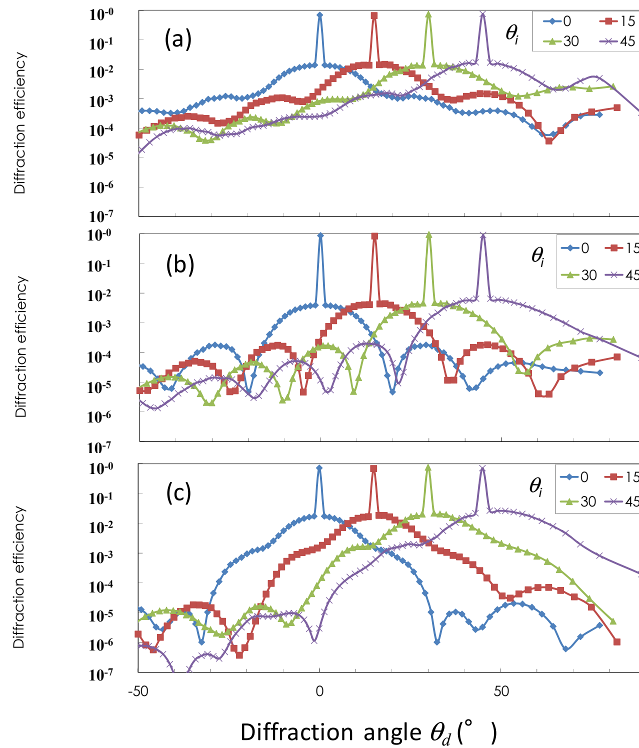

Fig. 9. Diffraction pattern of the particles with different incident angles. The widths and aspect ratio of the particles are changed. (a) The ellipsoidal particle has a width of 3λ and aspect ratio of 0.4. (b) The rectangular particle has a width of 3λ and aspect ratio of 0.2. (c) The triangular particle has a width of 5λ and aspect ratio of 0.2.

The diffraction pattern of particles P2–P5 are shown in Fig. 10. To ascertain the shapes and aspect ratios of these particles, the criterion given in Table 1 was used. This criterion is derived from the simulation (See appendix, Figs. 16–18 for case of TM mode). We can classify the shape into triangle, rectangle or ellipsoid, from the diffraction pattern with incident angle 0° and data of the other incident angle is not indispensable. As to triangle and ellipsoid, aspect ratio r_{asp} is also derived from the data at θ_i = 0° for one θ_r. As to rectangle, the diffraction pattern with incident angle 0° is not dependent on r_{asp} very much and we need another incident angle 45°.

Optics EXPRESS

The schematic procedure to decide the shape and size is as follows.

(1) Get the tentative width of the particle from Eq. (1) and decide θ_r for the cross section.

(2) Estimate the rough shape using Table 1.

(3) Perform additional measurement at $\theta_i = 45°$ for rectangle.

(4) Estimate the aspect ratio using Table 1.

In procedure (2), we selected the cross section whose width is the shorter, because the result is expected to be stable irrespective of deviation of beam spot from the center of the particle.

P2 and P5 may be rectangular as their patterns oscillate with a large amplitude. The diffraction pattern of a rectangle does not considerably change by the aspect ratio. Note that we used the experimental data of $\theta_i = 45°$ and compared the data with the corresponding simulation data. The polarization is TM, $w = 10\lambda$, 20λ, 30λ, 34λ, and 40λ, and $\theta_i = 45°$. (See appendix, Fig. 19 for cases $w = 10\lambda$ and 20λ). The difference between two peak angles decreases as r_{asp} increases at around $\theta_d = 0$.

The final results were compared with the image obtained from an optical microscope, as shown in Fig. 11. The projection image and cross-sectional shape are shown in the left column of each particle's pictures. Rhodamine B is purple and clearly seen.

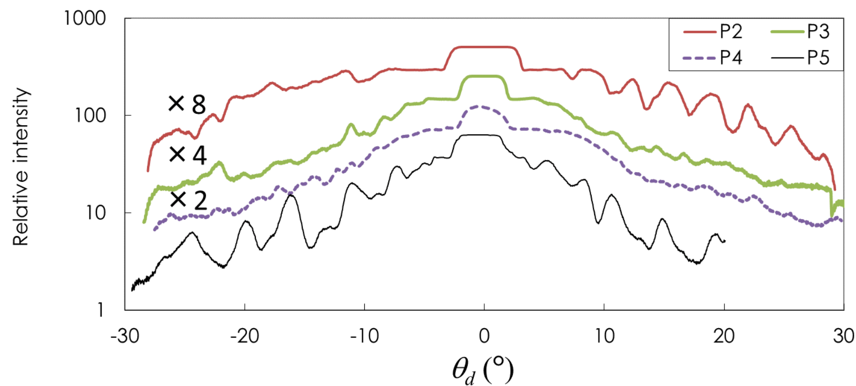

Fig. 10. Horizontal projection profiles of the diffraction patterns of particles P2–P5; $\theta_i = 0°$.

Table 1. Criterion to judge the shape and aspect ratio from the diffraction pattern

Scatterer	State of pattern	Aspect ratio dependency[a]
Rectangle	strong amplitude of oscillation	two peaks' angle difference for θ_i 45° is smaller
Ellipsoidal	weak amplitude of oscillation	declination of envelope is steeper
Triangle	large and broad two peaks	absolute angle of the broad two peaks is larger

[a]The tendency that occurs when the aspect ratio increases.

Optics EXPRESS

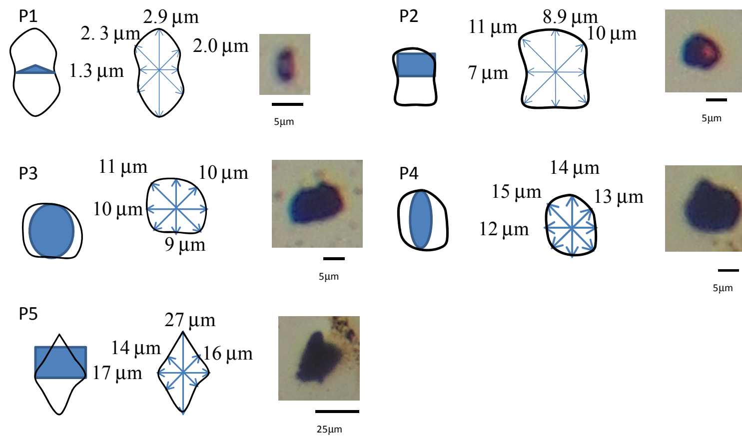

Fig. 11. Structures of the particles. The order of the images is—cross section, projected image, and microscopic image—from left to right. Cross sectional shape is added to the projected left images. The widths for four directions are indicated by bidirectional arrows in the middle images.

The number of peaks of the diffraction pattern changes with the shape (Table 2). Therefore, the width derived from Eq. (1) should be corrected. However, we did not consider this factor.

Table 2. Number of peaks. –50° < θ_d - θ_i < 0°. The width of particle is 20λ.

Shape	θ_i(°)	Aspect ratio: r_{asp}				
		0.2	0.4	0.6	0.8	1.0
Ellipsoidal	0	12.8	12.3	12.8	13.5	13.5
	15	13.5	13.5	13.5	13.5	13.0
	30	13.5	13.5	13.0	13.0	13.5
	45	13.0	13.5	13.0	12.0	13.3
Rectangle	0	12.8	12.3	13.3	13.5	13.5
	15	12.5	13.5	13.5	13.5	13.0
	30	13.5	13.5	13.0	13.0	13.5
	45	13.5	13.8	13.0	12.0	13.5
Triangle	0	7.0	9.0	9.5	11.5	12.0
	15	8.0	10.5	10.0	11.0	12.0
	30	9.5	8.0	10.0	11.5	9.0
	45	7.5	6.0	10.0	7.5	11.0

4. Discussion

Through pattern simulation, the shape of the cross section was determined from the amplitude of the fluctuation and the outline of the angular distribution. The aspect ratio was estimated from the space between the angles at the peaks or the declination of the angular distribution. For the rectangle, we also used the pattern for an incidence angle of 45° to estimate the aspect ratio. In Fig. 11, these results were compared with the microscopic images. In Fig. 10, the projection does not agree with the microscopic image very well. We believe that some of the reasons for this disagreement are as follows.

1. The peak interval in the angular distribution of a triangle differs from those of ellipsoid and rectangle (Table 2). This may affect the estimated particle width. The main pattern difference between an ellipsoid and a rectangle is the amplitude of fluctuation, which may due to the difference in edge sharpness of each shape. But, the peak interval does not differ between them a lot.

Optics EXPRESS

2. When we are to set the beam spot at the center of the particle, we think the condition was satisfied, if the diffraction pattern is symmetric (See Fig. 3(b)). The shape center is assumed to be the center of the diffraction pattern. The experimental setting of beam spot to the shape center is not difficult; however, it was not verified as the true center. The position of the diffraction center in *xy* plane was extremely sensitive that the precision seemed to be less than a few micrometers. However, the diffraction center may change if the particle shape is not symmetric. One of the reasons of above mentioned disagreement may be deviation of the tentative center from the real center.
3. The cross-sectional shape of the particles is assumed to be symmetric but may not be so as the diffraction pattern is asymmetric (Fig. 10). The deviation from the asymmetry was not treated in this study because the story becomes complex; however, this affects the diffraction pattern [28].
4. The ellipsoidal shape of the diffraction pattern in Fig. 3(b) is slanted. This tendency is the same for other particles. This may be due to the original beam shape, which is bended at 90° twice by reflection of the mirror, and the normal direction of the mirror surface is not in the plane including the two optical axes.
5. The refractive index of the particle is not 1.5 and has anisotropy by the molecular orientation [45]. Though the effect of refractive index difference 0.1 is not large, its effect cannot be neglected.

Thus, we listed five reasons for the experimental error. Reason (1) is the most important among them. The triangular particle's width might be estimated to be half of the real width (Table 2); however, Fig. 11 indicates that the other shape's widths do not differ much when they are compared with the microscopic results.

Next, we emphasize the focusing problem. In Figs. 4 and 6, the data intervals along the *z*-axis were set so that the pattern clearly changes. The interval of f_z in Figs. 2 and 4 is 100 μm, whereas that in Figs. 5 and 6 is 2.44 μm. This difference is partly due to the difference in size of the iris diaphragm. The aperture of the former (Fig. 2) is 1 mm (slit width) with a focal distance of 50 mm and ratio of 0.02. The ratio of the latter (Fig. 5) is 0.48. 0.48/0.02 is 24. The 24 times difference of NA explains the difference of the intervals 2.44μm and 100μm. In experiment, distance f_p adjustment was performed without the slit and the aperture was set 6mm. The variation of the contrast against f_p is the more sensitive. The difference of NA between the experiment and the simulation is due to the limitation of the simulation range by computer capacity. We were unable to considerably increase the focal length of the simulation.

Another possible reason for the difference of the intervals is the aberration along the optics axis. The fluctuation of the peak intensity by the variation of f_z might be averaged.

5. Conclusion

In this study, we developed a method to obtain various cross-sectional shapes of 3D particles by applying rigorous simulation to the cross-sectional diffraction pattern by using a 488 nm laser. Although we used the first-order approximation, we obtained an acceptable size and shape. The analyzed size was 2–20 μm and the shape was an ellipsoid, a rectangle, or a triangle with different aspect ratios. This technique is applicable to particles in the resonance domain with wavelength ranging from soft X-ray to microwave.

6. Appendix: Scattering pattern simulated using RCWA

The RCWA calculation results are shown in the appendix and their detailed calculation condition are stated in the main body.

Optics EXPRESS

The electric field of lens focusing on the particle is calculated by RCWA in Fig. 12. The lens with width 24μm condenses light and its focal spot is in front of the particle. Figs. 13 and 14 show that the contrast changes significantly against the distance f_z in this optical system. There is clearly unique f_z which gives the highest contrast whatever the shape of particle is circle or triangle.

Fig.15 shows that effect of thickness of the substrate is not critically important for calculating the diffraction pattern. Therefore, we don't have to use the real thickness of the substrate and can use the calculable thin thickness.

Figs. 16-19 give the criterion to judge the kind of shape of the particle from the diffraction pattern. Furthermore, they enable us to estimate the aspect ratio of the shape. The rectangle is difficult to estimate its aspect ratio from the diffraction pattern when the incident angle θ_i is 0°. Fig. 19 enables us to estimate the aspect ratio of rectangle by changing the incident angle.

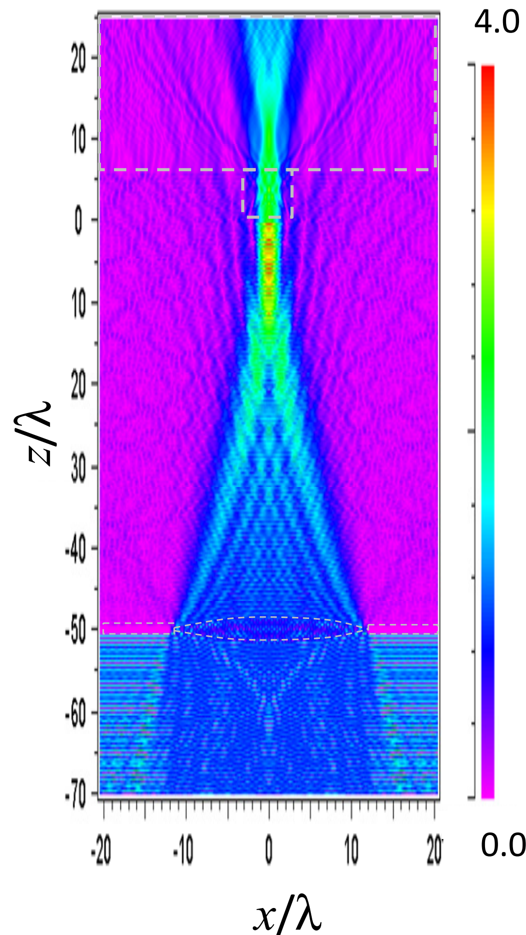

Fig. 12. The electric field of lens focusing in xz plane for TE mode. A lens and a square particle are indicated by dotted gray line.

Optics EXPRESS

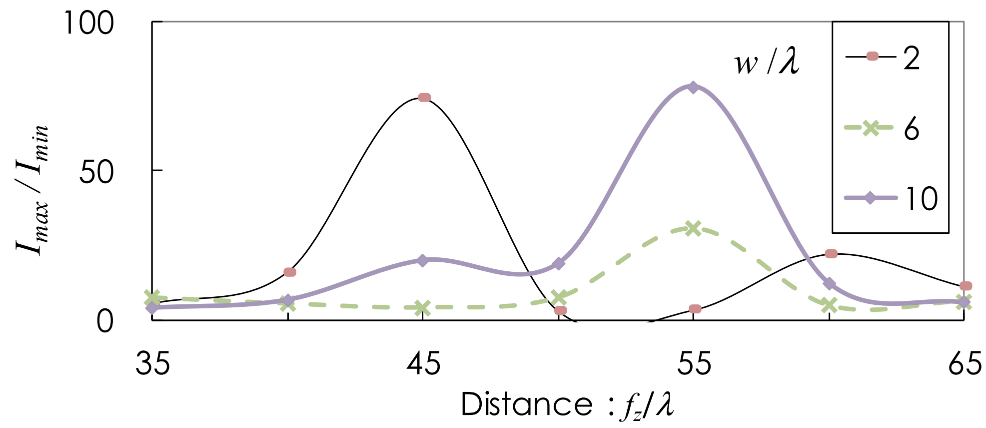

Fig. 13. Contrast derived from scattering pattern simulated using RCWA for a triangle. $w = 2\lambda$, 6λ and 10λ.

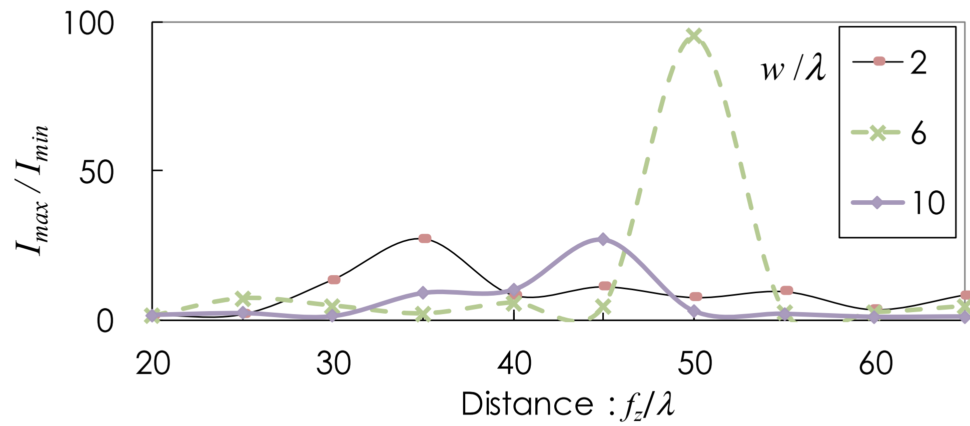

Fig. 14. Contrast derived from scattering pattern simulated using RCWA for a circle. $w = 2\lambda$, 6λ and 10λ.

Optics EXPRESS

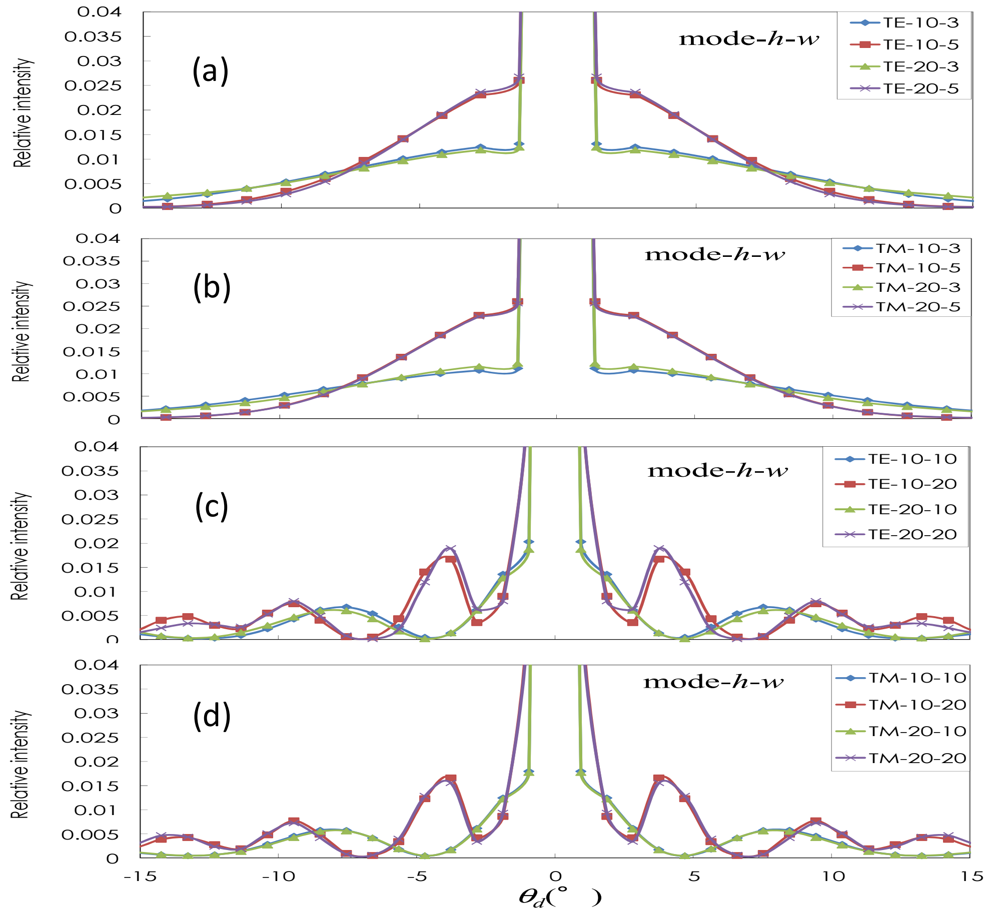

Fig. 15. The diffraction pattern of a circular particle. The unit is λ. (a)(b)(c)(d) Polarization, h and w are varied.

Optics EXPRESS

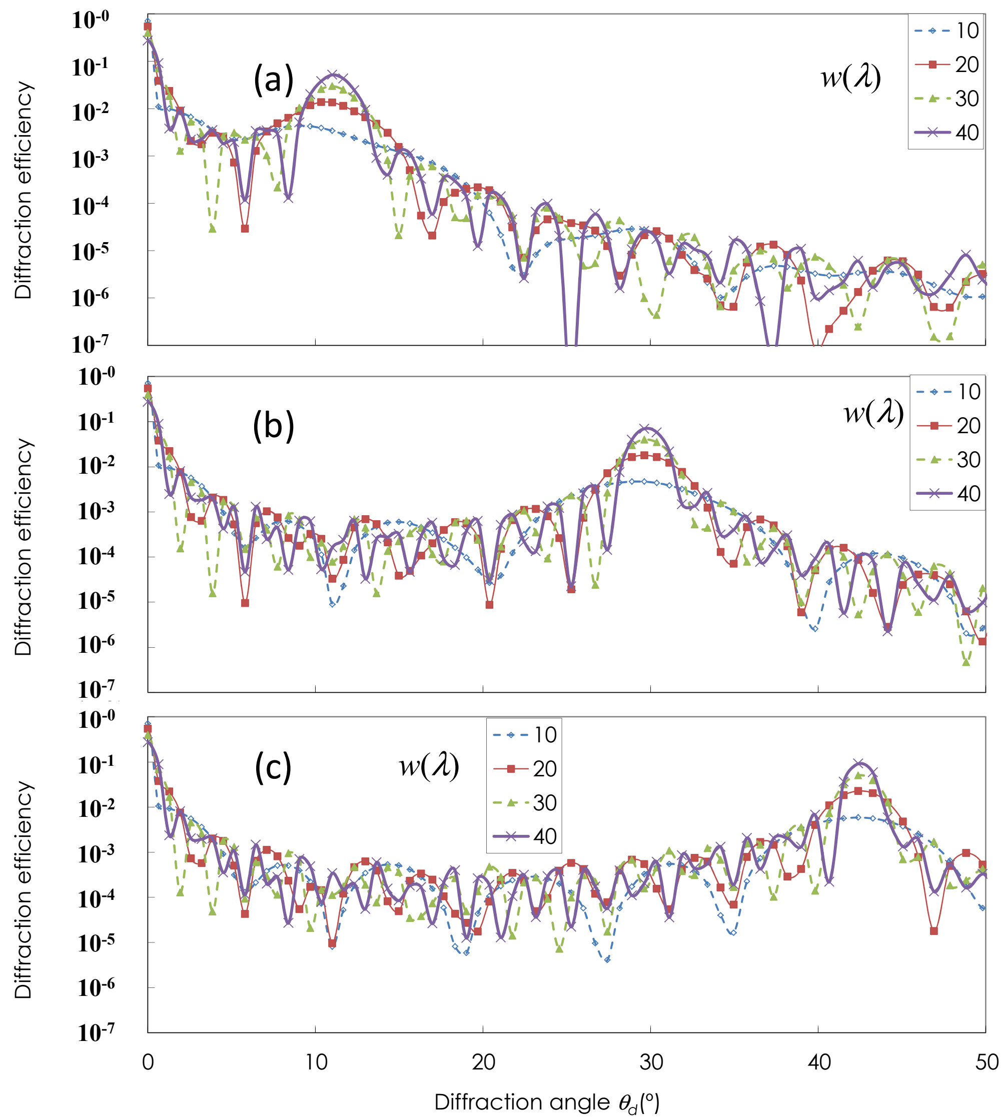

Fig. 16. The diffraction pattern of a triangular particle with different aspect ratio. Polarization is TM. (a) $r_{asp} = 0.2$. (b) $r_{asp} = 0.6$. (c) $r_{asp} = 1.0$.

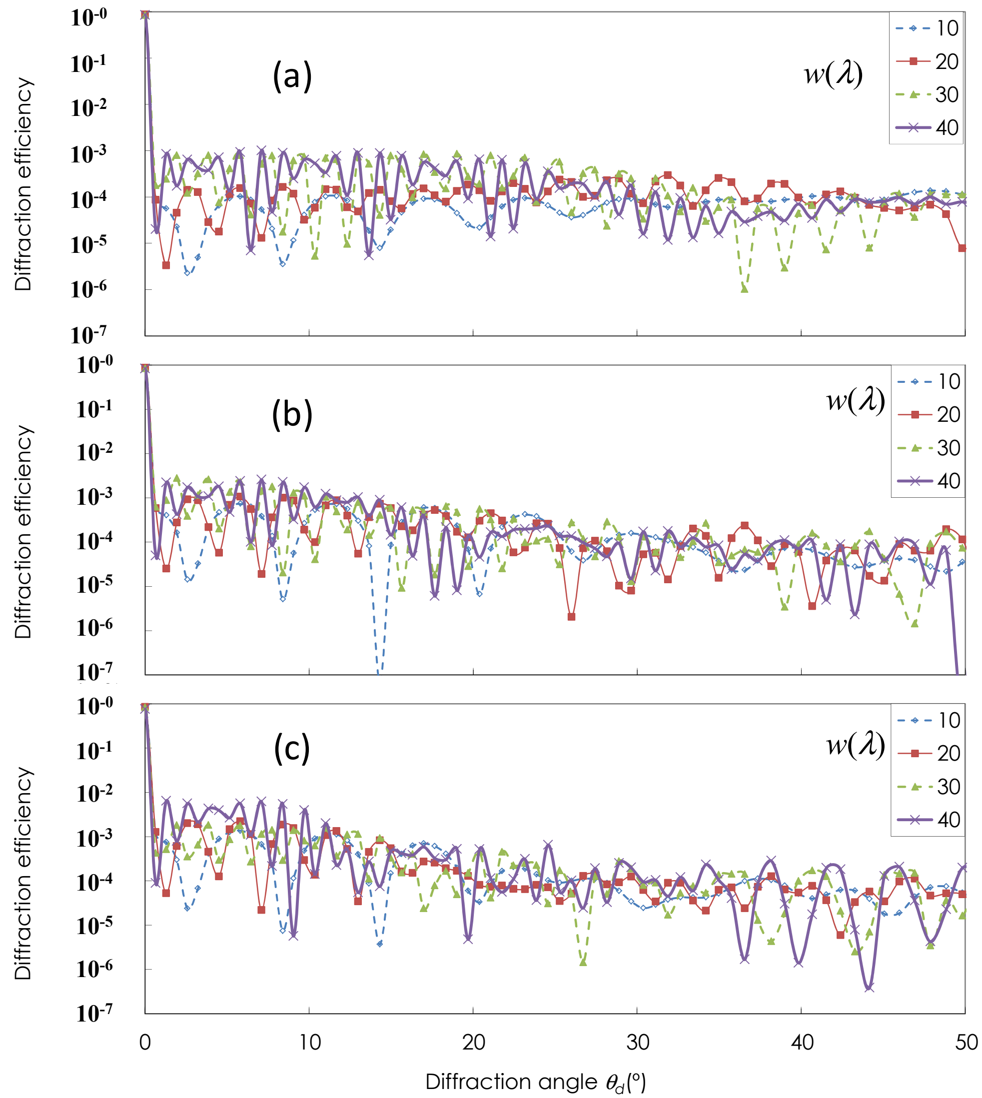

Fig. 17. The diffraction pattern of a rectangular particle with different aspect ratio. Polarization is TM. (a) r_{asp} = 0.2. (b) r_{asp} = 0.6. (c) r_{asp} = 1.0.

Optics EXPRESS

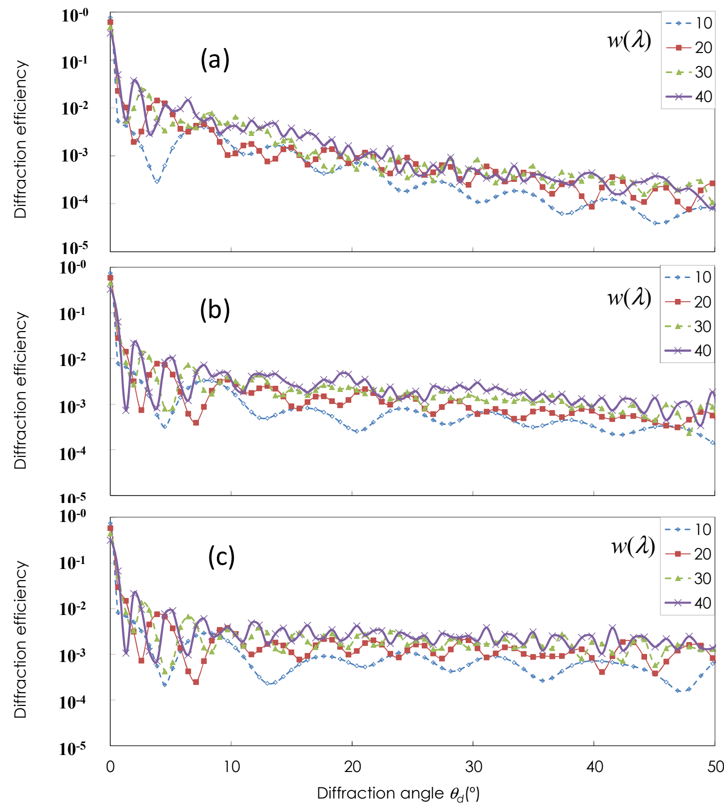

Fig. 18. The diffraction pattern of an ellipsoidal particle with different aspect ratio. Polarization is TM. (a) $r_{asp} = 0.2$. (b) $r_{asp} = 0.6$. (c) $r_{asp} = 1.0$.

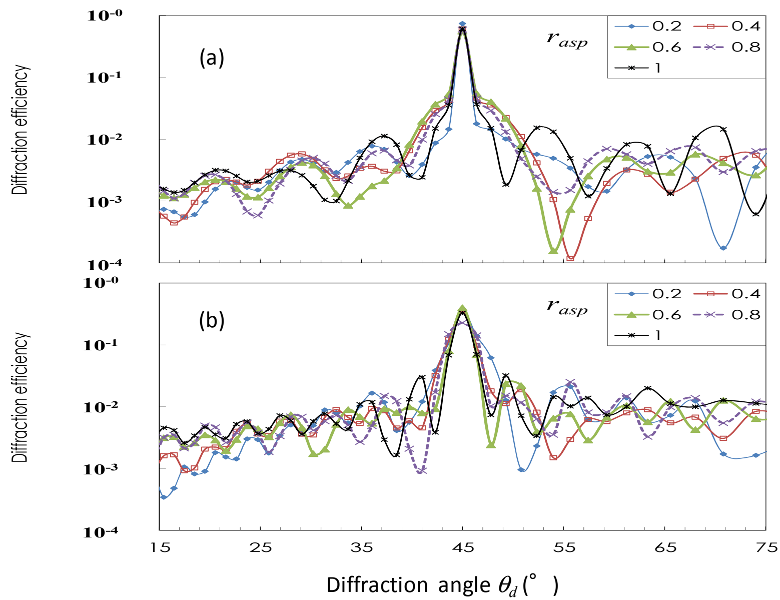

Fig. 19. The diffraction pattern of a rectangular particle with different aspect ratio. Polarization is TM. (a) $w = 10\lambda$. (b) $w = 20\lambda$.

Funding

JSPS KAKENHI (JP16K45678).

130.158.56.102 {ts '2017-11-15 21:45:48'}